Heliyon 9 (2023) e22674

Contents lists available at ScienceDirect

Heliyon

journal homepage: www.cell.com/heliyon

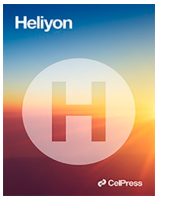

Detection of SARS-CoV-2 S protein based on FRET between carbon quantum dots and gold nanoparticles

Yang Li [a], Yashuang Ren [a], Zhihao Yi [a], Shitong Han [a], Shilei Liu [a], Feng Long [b], Anna Zhu [a,*]

[a] State Key Laboratory of NBC Protection for Civilian, Beijing, 102205, China
[b] School of Environment and Natural Resources, Renmin University of China, Beijing, 100872, China

ARTICLE INFO

Keywords:
SARS-CoV-2
Carbon quantum dots
Gold nanoparticles
Detection
FRET

ABSTRACT

The COVID-19 pandemic caused by SARS-CoV-2 virus brings nasty crisis for public health in the world. Until now, the virus has caused multiple infections in many people. Detecting antigen to SARS-CoV-2 is a powerful method for the diagnosis of COVID-19 and is helpful for controlling and stopping the pandemic. Herein, a rapid and quantitative detection method of SARS-CoV-2 spike (S) protein was built based on the fluorescence resonance energy transfer (FRET) phenomenon without complicated steps. In the process of detecting, the carbon quantum dots (CQDs) and gold nanoparticles (AuNPs) act as donor and acceptor. By modifying the SARS-CoV-2 antibodies on the surface of CQDs and AuNPs, we achieved S protein specific detection using the distance-based FRET phenomenon. Through the electric charge regulation, the limit of detection (LOD) is 0.05 ng/mL, the linear range is 0.1–100 ng/mL, and the detection process only takes 12 min. The proposed method exhibits several advantages such as be available for variants (B.1.1.529 and B.1.617.2) and be suitable for human serum, which is of significance for detecting viral in time and prevention the viral transmission.

1. Introduction

SARS-CoV-2 has affected people's health and normal life since it outbroke in 2019. It is highly contagious and spreads rapidly through human-to-human transmission or through aerosols spread. Rapid detection technologies for SARS-CoV-2 are prerequisite for timely blocking the spread of the virus and then for taking necessary antiviral measures. Up to now, reverse transcription-polymerase chain reaction (RT-PCR) is the gold standard for SARS-CoV-2 detection [1]. However, RT-PCR is a hard work that requires much more time and professional operation such as RNA extraction and reverse transcription steps, which will make it hard to achieve rapid on-site detection. Based on the above issues, rapid and simple detection technologies for SARS-CoV-2 antigen have drawn the attention of researchers [2,3].

As we all known, SARS-CoV-2 is a coronavirus named for its peripheral corona-like S proteins. These outwardly protruding S proteins bind to angiotensin-converting enzyme 2 (ACE2) on the inner track of the respiratory system and enter the human body. There are about 100 S protein trimer structures in a single virus [4]. Therefore, the S protein is a major antigen and target for human antibody binding to prevent its entry into host cells [5].

* Corresponding author.
E-mail address: chuanna0306@163.com (A. Zhu).

https://doi.org/10.1016/j.heliyon.2023.e22674
Received 11 July 2023; Received in revised form 16 November 2023; Accepted 16 November 2023
Available online 19 November 2023

Carbon quantum dots (CQDs) are typical zero-dimensional carbon materials with the advantages of strong fluorescence intensity, low toxicity, good performance of chemical stability and biocompatibility, high electron transfer efficiency, and high quantum yield [6–9]. In addition, CQDs can be easily synthesized [10,11], and have many functional groups such as carboxyl, carbonyl, hydroxyl, etc. CQDs can be further modified conveniently [12,13] and used as energy donors in the process of immune reaction. At present, the detection of SARS-CoV-2 antibodies using graphene quantum dots based on FRET has been reported [14]. To the best of our knowledge, the S protein detection utilize the carbon quantum dots (CQDs) has not been reported.

Noble metal nanoparticles such as gold nanoparticles have remarkable plasmonic, catalytic and electronic properties. Gold nanoparticles are very biologically inert, so they are suitable for protein immobilization without protein denaturation. Therefore, gold nanomaterials are commonly used in virus detection, including the SARS-CoV-2 detection, such as lateral flow immunoassay (FLIA) [15,16], surface plasmon resonance (SPR) [17,18], surface-enhanced Raman spectroscopy (SERS) [19], etc. Light-induced excitation of conduction electrons can drive the localized surface plasmon resonance (LSPR) phenomenon of AuNPs, which is a characteristic optical property of AuNPs. Strong optical absorption may occur at characteristic frequencies in the region of visible light to near infrared light, therefore AuNPs are often used as FRET acceptors for biosensors [20,21].

The aim of this study is to develop a sensitivity, fast and convenient method for SARS-CoV-2 antigen detection based on "turn-off-on" fluorescence mode. Enable to apply the "turn-off-on" mode, the donor and acceptor must be close enough, so the electric charge regulation strategy was proposed. The negatively charged AuNPs (presented as$_{-}$AuNPs) and positively charged AuNPs (presented as$_{+}$ AuNPs) were synthesized, and when necessary, the antibodies were modified on the surface of AuNPs (presented as AuNPs-Ab) for further investigations. The antibodies were modified on the surface of CQDs (presented as CQD-Ab) and then were served as energy donor. When S proteins are present in the system, the distance between the donor and the acceptor increases due to the immune reaction between the monoclonal antibody and the antigen, thus affecting the FRET between CQDs and AuNPs. The principle is based on the classical theory that distance affects energy transmission efficiency [22–24]. It was proved that the best detection results could be obtained when + AuNPs were used as energy acceptors and the CQDs-Ab were used as energy donors. Finally, we developed a novel FRET biosensing detection methods, the proposed method exhibits many advantages including high sensitivity (LOD is 0.05 ng/mL), quick detection (detection time is 12 min), easy operation and high specificity. This research has great potential for SARS-CoV-2 virus early diagnosis and preventing disease transmission.

2. Materials and methods

2.1. Materials and reagents

The PBS buffer (50 mmol/L, pH = 7.4), EDC (N-(3-Dimethylaminopropyl)-N′-ethylcarbodiimide hydrochloride, 98.5 %), Sulfo-NHS (N-hydroxysulfosuccinimide, ≥99.9 %), BSA (bovine serum albumin, ≥98 %) were purchased from Shanghai Macklin Biochemical Co., Ltd. (Shanghai, China). The MES buffer (0.1 mol/L, pH = 5.5) was purchased from OKA Biotechnology Co., Ltd. (Beijing, China). The cysteamine (95 %), chloroauric acid (98 %), sodium citrate (99 %) were purchased from Shanghai Acmec Biochemical Co., Ltd. (Shanghai, China). Sodium borohydride was purchased from Sinopharm Chemical Reagent Co., Ltd. (Shanghai, China). Carbon Quantum Dots were purchased from Suzhou Xingshuo Nanotech Co., Ltd. (Suhou, China). Anti-SARS-CoV-2 spike RBD neutralizing antibody, SARS-CoV-2 trimer S protein, Delta variant trimer S protein (B.1.617.2), Omicron variant trimer S protein (B.1.1.529) were purchased from ACROBiosystems Co., Ltd. (Beijing, China). The human serum was purchased from Guangzhou Hongquan Biotechnology Co., Ltd. (Guangzhou, China). The ultrafiltration centrifuge tubes (Millipore, Ultra-15 mL, 30 kDa Centrifugal Filter Unit, USA) were used.

2.2. Equipment

Fluorescent spectrometer (Edinburgh Instruments FLS 1000, UK), UV/VIS spectrophotometer (Agilent Cary 60, US), high-speed freezing centrifuge (Sigma 3K15, US), nanoparticle size and Zeta potential analyzer (Malvern Zetasizer Nano-ZS ZEN3600, UK), transmission electron microscope (TEM Hitachi HT7800, Japan), fourier transform infrared spectrometer (FTIR Thermo Scientific Nicolet iS50, US), X-ray photoelectron spectroscopy (XPS Thermo Scientific K-Alpha Nexsa, US), heating magnetic stirrer (IKA RCT basic, Germany).

2.3. Synthesis of negatively charged AuNPs

Negatively charged gold nanoparticles (here presented as $_{-}$AuNPs) were prepared with the reduction method using chloroauric acid and sodium citrate [25]. The procedure is as follows: All the glassware to be used were washed with acid and deionized water. Add 198 mL ultrapure water and 2 mL 1 % chloroauric acid solution into a flat-bottomed conical flask to make the concentration of chloroauric acid to 0.01 % (w/V). Put the flask onto a magnetic stirrer and then set the stirring speed to 600 rpm and the temperature to 100 °C. 4 mL of 1 % sodium citrate solution was quickly added into the flask after the liquid was boiled, and then let the mixture react for 10 min. After that, wine-red negatively charged gold nanoparticles ($_{-}$AuNPs) were obtained and then store at 4 °C.

2.4. Synthesis of positively charged AuNPs

Positively charged gold nanoparticles (here presented as $_{+}$AuNPs) were prepared based on the methods described in literatures

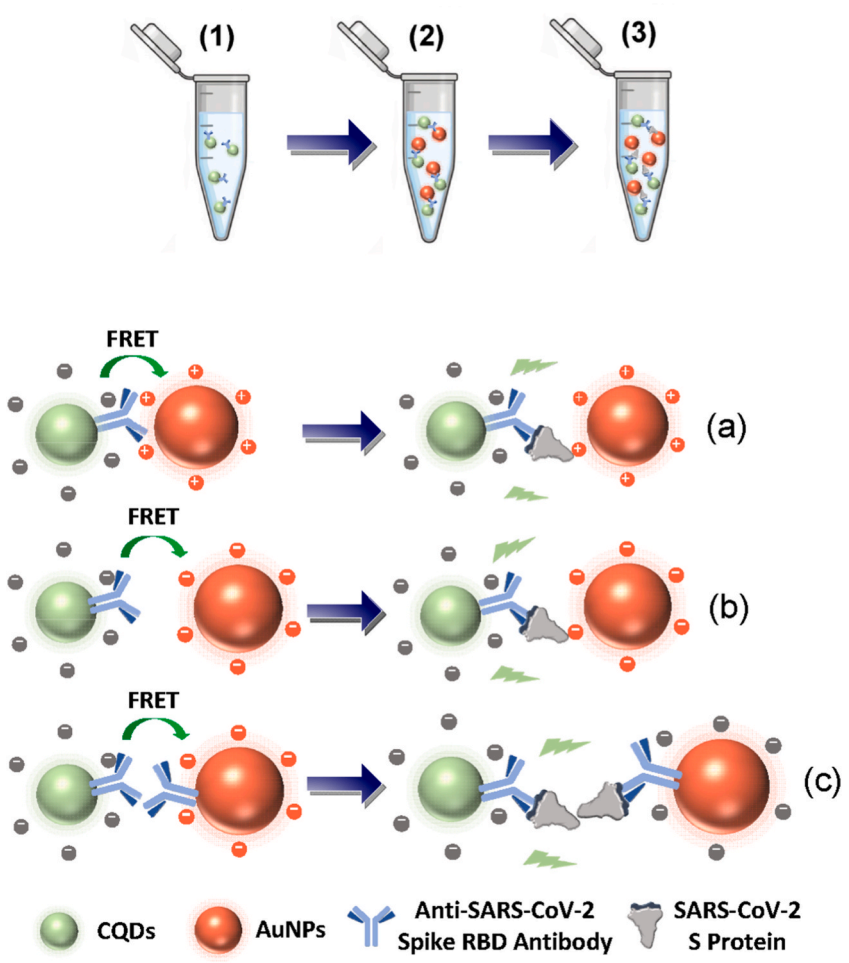

Fig. 1. FRET fluorescence detection steps.

[26–28] but with slight changes. Chloroauric acid and sodium borohydride were used to react in the dark at room temperature, and cysteamine was added to coat the surface of AuNPs with amino groups to obtain a positively charged state. The procedure is as follows: 500 μL 216 mmol/L of cysteamine solution were added into 200 mL 0.01 % (w/V) chloroauric acid solution, and then stirring for 20 min at 400 rpm under room temperature. Later, quickly add 10 μL 10 mmol/L sodium borohydride solution, set the stirring speed to 500 rmp and then stirring vigorously for 15 min. Finally, wine-red positively charged gold nanoparticles (+AuNPs) were obtained and stored at 4 °C.

2.5. Preparation of antibody conjugated CQDs

The EDC-NHS covalent chemistry was used to prepare the antibody conjugated CQDs (here presented as CQDs-Ab). Firstly, 100 μL 10 mg/mL CQDs solution was diluted to 5 mL with MES buffer (pH = 5.5). Then add 0.8 mg EDC and 2.2 mg Sulfo-NHS, and react for 15 min. Add 1.5 mL PBS (pH = 13) to adjust the solution pH to 7.6. Next, 200 μL 0.2 mg/mL anti-SARS-CoV-2 spike RBD neutralizing antibodies were added and react for 2 h. Add 200 μL 2 mg/mL BAS solution and wait for 30 min to block the non-specific adsorption sites. Centrifugate the mixture in 30 kDa ultrafiltration centrifuge tube for 10 min (set RCF to 3743 g and temperature to 4 °C). Finally, the unconjugated CQDs were filtered out and 2 mL CQDs-Ab solution was obtained.

2.6. Preparation of antibody conjugated AuNPs

According to the strong coordination of gold-sulfur bonds, antibody conjugated gold nanoparticles can be prepared by the method of thiol ligand exchange. 10 mL+AuNPs (or -AuNPs) solution was mixed with 200 μL 0.2 mg/mL anti-SARS-CoV-2 spike RBD neutralizing antibody and react for 24 h. Centrifugate the solution as depicted in section 2.5 to filter out the unconjugated AuNPs. Finally, 5 mL +AuNPs-Ab or -AuNPs-Ab were obtained.

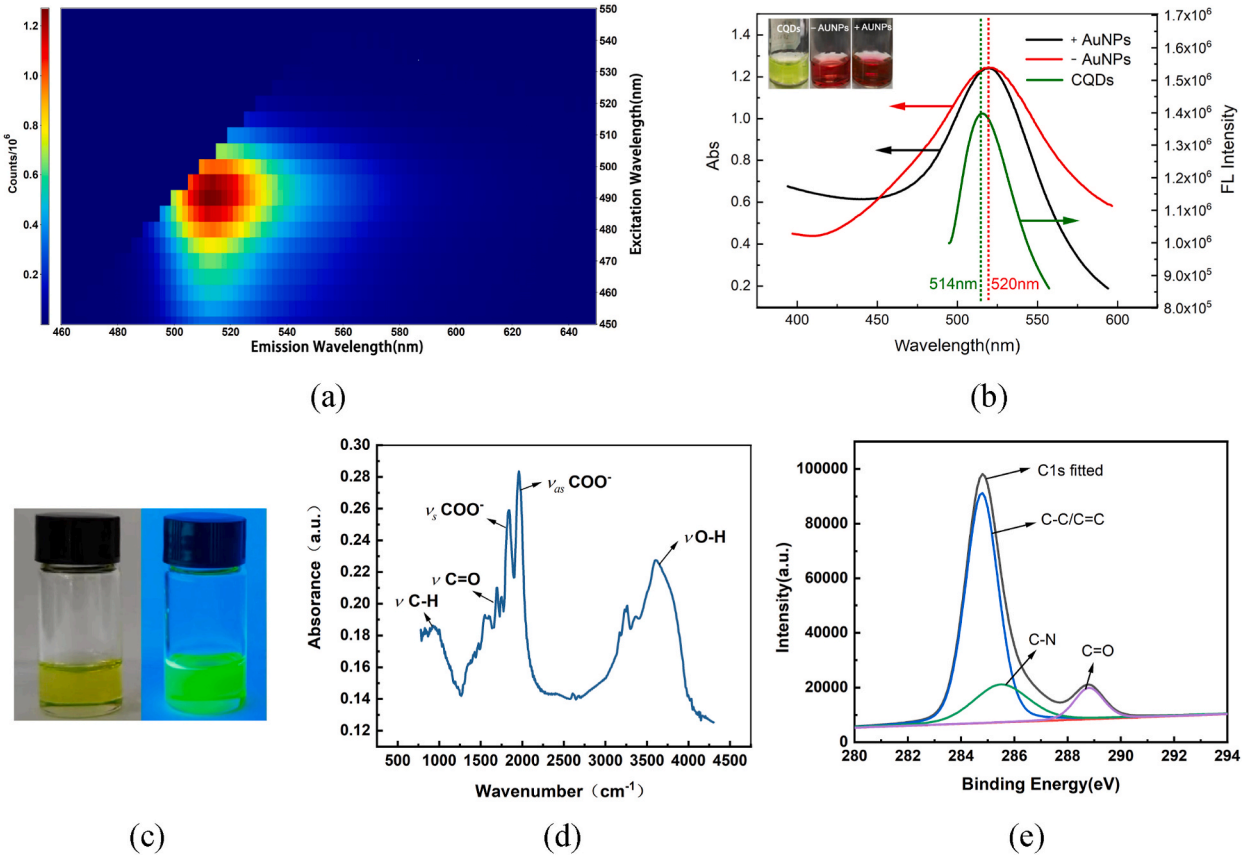

Fig. 2. The fluorescence of CQDs and ultraviolet absorption of AuNPs. (a) Full scan of the excitation and emission wavelengths of the CQDs, (b) Ultraviolet absorption of AuNPs and fluorescence emission of CQDs, (c) The green fluorescence of the CQDs, (d) FTIR spectra of CQDs, (e) The XPS deconvoluted spectra of C1s.

2.7. Zeta potential and TEM testing

The Zeta potential analyzer and transmission electron microscope (TEM) were utilized to characterize the CQDs, -AuNPs, +AuNPs, COQs-Ab and AuNPs-Ab.

2.8. The S protein detection

The detection process is shown in Fig. 1. First, a certain volume of CQDs-Ab was added into a 1.5 mL centrifuge tube. Next, a certain volume of AuNPs was added, including +AuNPs, -AuNPs, +AuNPs-Ab or -AuNPs-Ab. After stable for a short time, when CQDs-Ab and AuNPs were tightly adsorption, the fluorescence intensity was measured as baseline value. Then add 50 μL S protein samples of different concentration and measure the fluorescence intensity after incubation for 10 min. Three pairs of donor and acceptor were prepared and used in our experiments. Fig. 1(a) shows the combination of CQDs-Ab/+AuNPs, Fig. 1(b) is the CQDs-Ab/-AuNPs, and Fig. 1(c) is the CQDs-Ab/±AuNPs-Ab. To avoid misunderstanding, when +AuNPs or -AuNPs were modified with antibodies, the similar characteristics were exhibited. So the +AuNPs-Ab or -AuNPs-Ab were defined as ± AuNPs-Ab.

3. Results and discussion

3.1. Absorption and fluorescence spectrum

In Fig. 2(a), a full scan of the excitation and emission wavelengths of the CQDs was performed. It can be seen that the maximum excitation wavelength of CQDs is 490 nm and the fluorescence emission peak is 514 nm. The fluorescence of the CQDs is green as illustrated in Fig. 2(c) and the quantum yield is 71.83 % in Fig. S5. In Fig. 2(b), both +AuNPs and -AuNPs have strong ultraviolet absorption peaks at 520 nm, and the absorbance values are similar, which is 1.24. It can be attribute to the localized surface plasmon resonance (LSPR) of AuNPs caused by electron cloud resonance on particle surface [29]. On the other hand, CQDs have the fluorescence emission peak of 514 nm, so the fluorescence resonance energy transfer (FRET) of AuNPs and CQDs would be achieved.

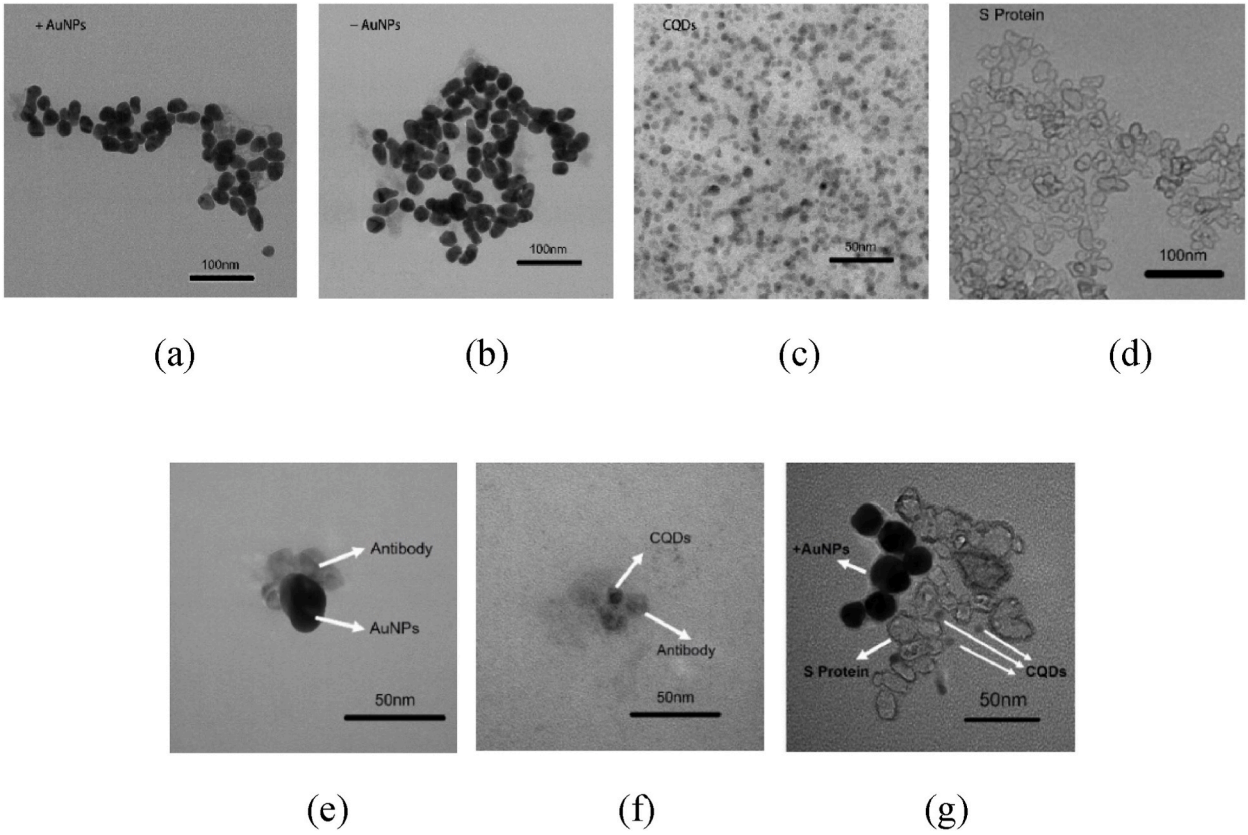

Fig. 3. TEM image of (a) +AuNPs, (b) -AuNPs, (c) CQDs, (d) S protein trimer structure of SARS-CoV-2, (e) AuNPs modified with monoclonal antibody, (f) CQDs modified with monoclonal antibody, (g) +AuNPs, CQDs-Ab and S protein.

According to the Lambert-Beer theory $c = A\ (e{\cdot}b)^{-1}$ [30], where c is the concentration of AuNPs, A is the absorbance value of the maximum absorption peak, $e = 2.7 \times 10^8\ M^{-1}cm^{-1}$ represent the extinction coefficient and $b = 1$ cm represent the length of the cuvette. According to this, it can be deduced that the concentration of +AuNPs and -AuNPs were 4.59 nmol/L.

The functional groups of the CQDs were also investigated by fourier transform infrared spectroscopy (FTIR) and X-ray photoelectron spectroscopy (XPS) analysis. As shown in Fig. 2(d), the band about 3200~3600 cm^{-1} was assigned to the stretching vibration of O–H bonds. The band about 1700~1800 cm^{-1} was confirmed to be –COOH, it is mainly caused by C═O stretching vibration. The measured C1s spectra for CQDs were deconvoluted and displayed in Fig. 2(e). The deconvolution shows the presence of C═C/C–C at 284.6 eV, C–V at 285.1 eV and C═O at 288.2 eV, which are consistent with the reported values [31,32]. These results suggested that the CQDs were full of oxygen-containing functional groups, which makes the CQDs available bound to antibodies [33]. In addition, the average lifetime values of the CQDs in the presence and absence of AuNPs were calculated. The lifetime spectra in Fig. S4 were fitted by Eq. (1), it is a double exponential decay equation. The average lifetime (τ_{ave}) was calculated according to Eq. (2).

$$I(t) = I_0 + A_1 \exp(-t/\tau_1) + A_2 \exp(-t/\tau_2) \tag{1}$$

$$\tau_{ave} = \left(A_1\tau_1^2 + A_2\tau_2^2\right) / \left(A_1\tau_1 + A_2\tau_2\right) \tag{2}$$

The average FL lifetime τ_C of the CQDs was 4.87 ns, the average FL lifetime τ_A when added +AuNPs was reduced to 2.14 ns. This demonstrates that the FL quenching mechanism is a dynamic quenching process and the FRET process between the CQDs and AuNPs was also confirmed [32]. Futher more, the FRET efficiency were calculated according to Eq. (3). Thus, the FRET efficiency is 56.06 %. The FRET distance *r* is about 50.5 Å, see Supplementary Material for details.

$$E = 1 - (\tau_A / \tau_C) \tag{3}$$

3.2. Characterized by TEM

Fig. 3(a), (b), (c) and (d) are the TEM image of the prepared +AuNPs, -AuNPs, CQDs and S protein respectively. From the particle size statistics, it can be seen from Fig. S1(a) that the average particle size is 21.8 nm. Fig. S1(b) is the -AuNPs with an average particle size of 21.6 nm. Fig. S1(c) shows the TEM image of CQDs with an average particle size of 7.7 nm. Fig. S1(d) illustrated the S protein trimer

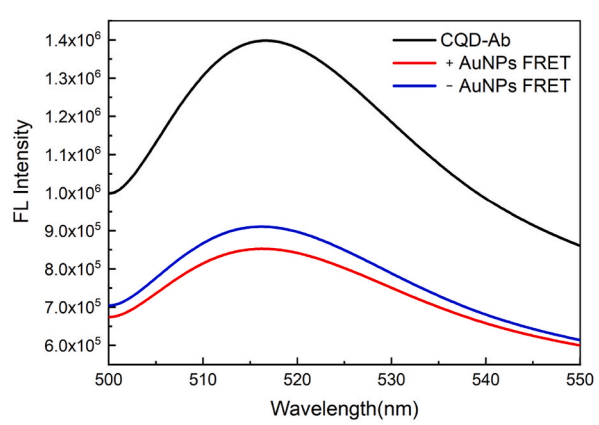

(a)

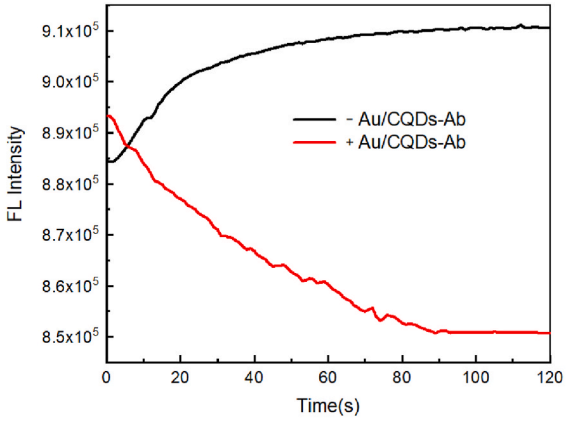

(b)

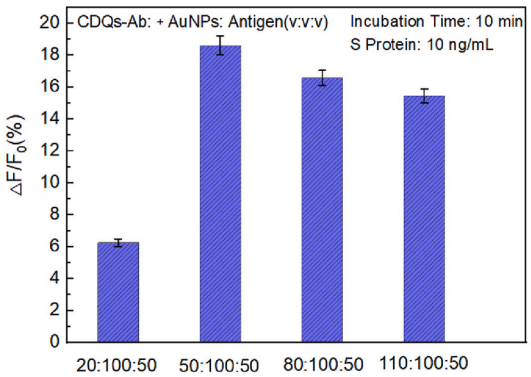

(c)

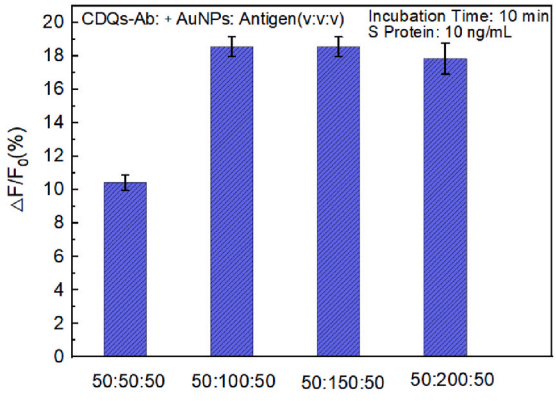

(d)

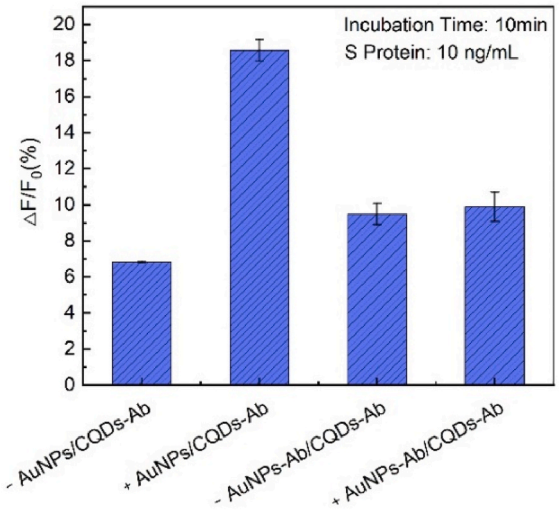

(e)

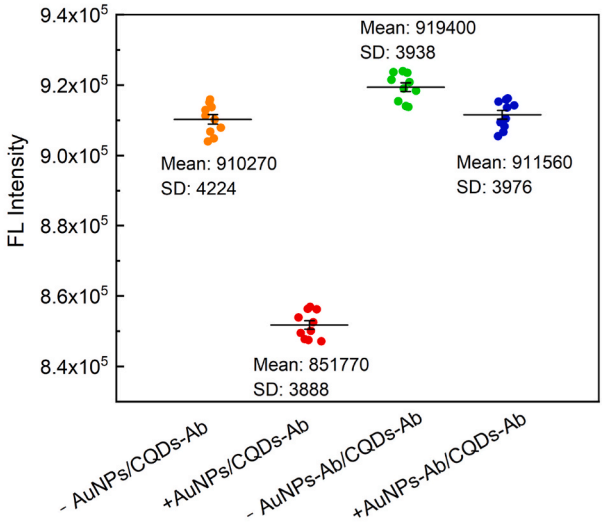

(f)

Fig. 4. Optimize detection conditions.(a) FRET between CQDs-Ab and AuNPs, (b) Fluorescence dynamic process, (c) and (d) Fluorescence increase rate at different dosage of CQDs-Ab, S Protein and +AuNPs, (e)The fluorescence increase of different acceptor-donor pairs, (f) The LOD calculate.

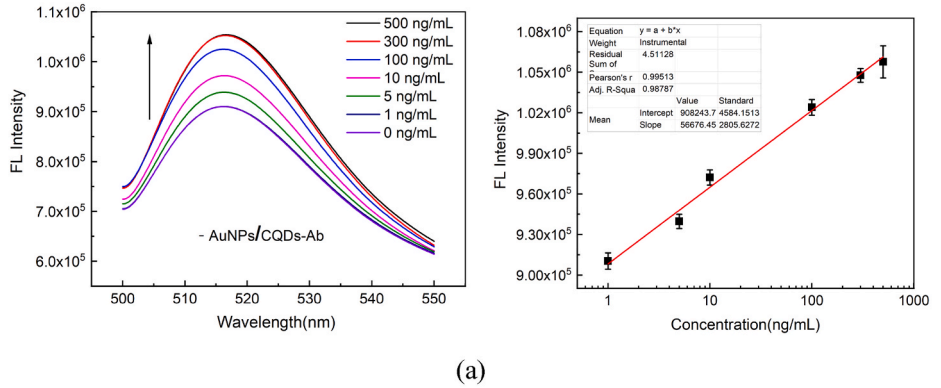

(a)

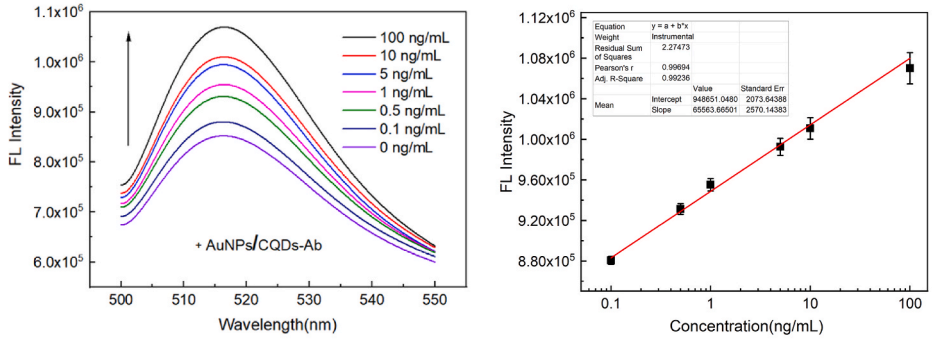

(b)

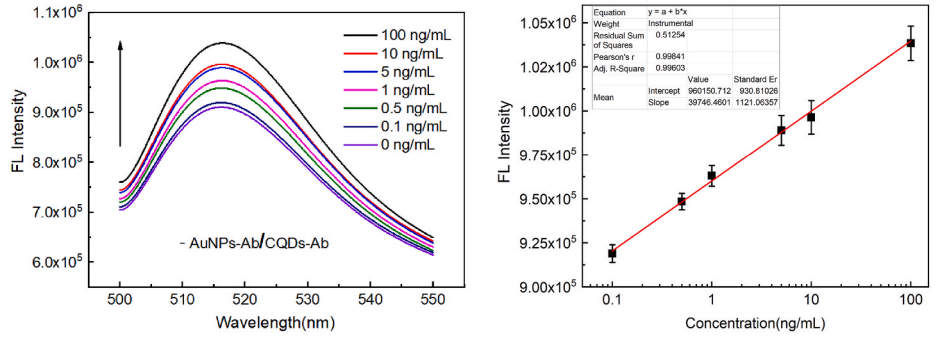

(c)

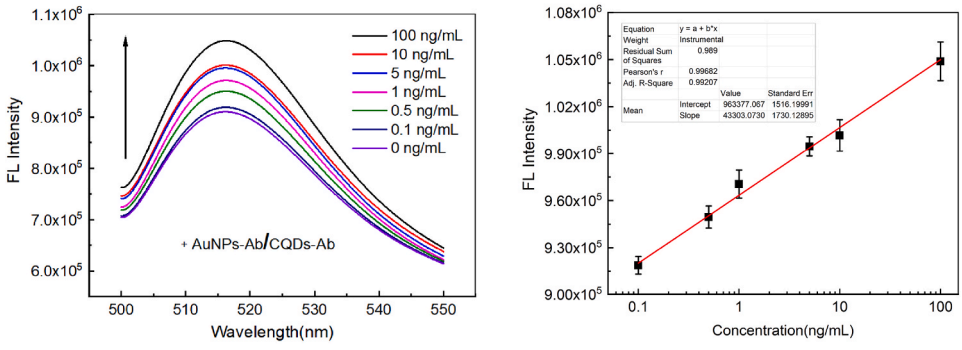

(d)

Fig. 5. The fluorescence intensity and standard curve of S Protein detection.

structure photographed by the negative staining technique and the size of each S protein trimer is approximately 15.7 nm. Fig. 3(e) and (f) shows the AuNPs and CQDs conjugated antibodies, in which the presence of antibodies can be observed, demonstrating that the antibody has been successfully conjugated. In Fig. 3(g), it can be seen that ₊AuNPs, CQDs-Ab and S protein are tightly adsorbed.

3.3. Zeta potential

The Zeta potential of CQDs, CQDs-Ab, ₋AuNPs, ₊AuNPs, ₋AuNPs-Ab and ₊AuNPs-Ab were tested. It can be seen from Fig. S2 that the Zeta potentials of ₊AuNPs and ₋AuNPs were 24.33 mV and −16.57 mV respectively, which proved the successful synthesis of positively and negatively charged AuNPs. The CQDs is negatively charged due to the carboxyl groups or other groups, with a Zeta potential of −6.5 mV. The Zeta potentials of CQDs-Ab, ₋AuNPs-Ab and ₊AuNPs-Ab are −12.30 mV, −10.67 mV and −10.72 mV respectively, which may be caused by the negative charges on the antibody surface.

3.4. FRET of AuNPs and CQDs-Ab

Take 50 μL CQD-Ab solution and add 450 μL PBS (pH = 7.4) solution. As can be seen from Fig. 4(a), the CQD-Ab fluorescence intensity is 1.4×10^6 be defined as F_0. Take 50 μL CQD-Ab, add 100 μL ₊AuNPs or ₋AuNPs, then add 350 μL PBS solution, the fluorescence intensities of ₊AuNPs and ₋AuNPs after FRET are 8.5×10^5 and 9.1×10^5, respectively. The fluorescence intensities after added AuNPs be defined as F_1. Then quenching efficiency can be can be calculated according to $(F_0–F_1)/F_0$. The quenching efficiency of ₋AuNPs and ₊AuNPs are 35 % and 39 %. Since the prepared CQD-Ab is negatively charged, ₊AuNPs can better adsorb and bind to CQD-Ab, the FRET effect is better. For a better illustrating of the FRET process, the fluorescence intensity was dynamically scanned after adding AuNPs. As shown in Fig. 4(b), the fluorescence signal was gradually rising when ₋AuNPs was added. This proved the repulsion process between CQD-Ab and ₋AuNPs. On the other hand, the fluorescence decreased was observed when ₊AuNPs was added. This is because the CQD-Ab and ₊AuNPs would attract each other and a better FRET phenomenon would be acquired, which attribute to the opposite electric charges. 2 min later, the fluorescence intensity was stabilized at 9.1×10^5 (CQDs-Ab/₋AuNPs) and 8.5×10^5 (CQDs-Ab/₊AuNPs), respectively. So the regulation effect of electric charges on FRET was proved and a stable time of 2 min was necessary as indicated in Fig. 1 step (2).

3.5. AuNPs and CQDs-Ab dosage optimization

Since it has been demonstrated that ₊AuNPs has better FRET effect, ₊AuNPs/CQDs-Ab was used as acceptor-donor combination to verify the used dosage. The volume of CQDs-Ab were 20 μL, 50 μL, 80 μL, and 110 μL, respectively. Then 100 μL ₊AuNPs and 50 μL S protein were added. Finally, PBS solution (pH = 7.4) was added to make up the volume to 500 μL. The fluorescence intensity was measured after 10 min incubation. It can be seen from Fig. 4(c) that when the CQDs-Ab:₊AuNPs:Antigen (v:v:v) = 50:100:50, the maximum fluorescence increase rate $\triangle F/F_0 = 18.6$ % can be obtained. Therefore, 50 μL CQDs-Ab and 50 μL antigen were used to investigate the optimal dosage of ₊AuNPs. As shown in Fig. 4(d), when the dosage of ₊AuNPs is 100 μL, a better effect can be obtained. Therefore, the optimal dosage of CQDs-Ab, ₊AuNPs and Antigen are 50 μL, 100 μL and 50 μL.

3.6. Detection of S protein by FRET

As illustrated in Fig. 1, three pairs of donor and acceptor were applied. From the conclusion of Fig. 4(b), it would be stabled for 2 min after the donor and acceptor were added. Then added antigen and incubated for 10 min to investigate the relationship between different antigen concentrations and fluorescence intensities. Fig. 5(a), (b), (c) and (d) are the fluorescence spectra and standard curves of different AuNPs and CQDs-Ab pairs, the R^2 of each standard curve can reach more than 0.99, and the linear relationship is perfect. As shown in Fig. 4(e), the fluorescence increase rate $\Delta F/F_0$ of ₋AuNPs/CQDs-Ab, ₊AuNPs/CQDs-Ab, ₋AuNPs-Ab/CQDs-Ab, and ₊AuNPs-Ab/CQDs-Ab are 6.8 %, 18.6 %, 9.5 % and 9.9 %, respectively (S protein concentration is 10 ng/mL, incubation time is 10 min). From Fig. 4(f), the LOD of each pair was calculated according to the mean value of blank sample plus 3 times SD (n = 10) [34]. The LOD result of ₋AuNPs/CQDs-Ab, ₊AuNPs/CQDs-Ab, ₋AuNPs-Ab/CQDs-Ab, and ₊AuNPs-Ab/CQDs-Ab are 1.82 ng/mL, 0.05 ng/mL, 0.19 ng/mL, and 0.12 ng/mL, respectively. Obviously, the pair ₊AuNPs/CQDs-Ab has the maximal $\Delta F/F_0$ and the best LOD, this attribute to the opposite electric charges between ₊AuNPs and CQDs-Ab so as to make them adsorbed with each other tightly. So the better FRET effect would lead to a better detection result. The pair ₋AuNPs/CQDs-Ab has the minimum $\Delta F/F_0$ and the worst LOD, this is because the same electric charges of ₋AuNPs and CQDs-Ab, which would keep them away from each other and then resulting the poor FRET effect. When ₋AuNPs or ₊AuNPs were conjugated to antibodies, their electrical charges would be converted to negatively and the Zeta potential almost the same. The Zeta potential of ₋AuNPs-Ab or ₊AuNPs-Ab depend on the antibodies. As Fig. 1(c) illustrated, ₋AuNPs-Ab or ₊AuNPs-Ab increased the probability of antigen adsorption, and the spatial distance is greater than that of ₋AuNPs/CQD-Ab due to the adsorption of double antigens, so its $\Delta F/F_0$ and LOD was better than ₋AuNPs/CQD-Ab.

For the ₊AuNPs/CQD-Ab, the total detection time was 12 min (including stabilization and incubation time), the LOD was 0.05 ng/mL, and the linear range was 0.1–100 ng/mL. Other S protein detection methods were summarized in Table 1, it can be seen that the LOD and detection time of this study are acceptable. The most important of all, our method has successfully combined the detection time and the detection sensitivity. This research has the advantages of convenient operation and has the potential for large-scale applications.

Table 1
The antigen detection methods.

LOD	Antigen	Method	Time	References
5 μg/mL	S1	Lateral Flow Assay LFA	30 min	[35]
0.11 ng/mL	S	Lateral Flow Assay LFA	30 min	[36]
0.033 ng/mL	S1	LFA, Fluorescence	30 min	[37]
0.1 ng/mL	S	LFA, Chemiluminescence	16 min	[38]
0.1 ng/mL	S	Fiber-optic	20 min	[39]
87.5 ng/mL or 2.5 ng/mL	S or N	FRET	1 min	[40]
0.05 ng/mL	S	FRET	12 min	This work

Table 2
Recovery of S protein in serum samples.

Added (ng/mL)	Found (n = 3, ng/mL)	SD	RSD (%)	Recovery (%)
0.1	0.115	0.013	10.84	115.45
1	1.151	0.148	12.83	115.10
10	11.005	1.463	13.30	110.05

3.7. Specificity of detection

In order to test the detection ability of this method for other variants, ₊AuNPs/CQD-Ab was used to detect wild-type, Omicron variant (B.1.1.529), Delta variant (B.1.617.2), S protein trimer structure of SARS and MERS. From Fig. S3, the $\Delta F/F_0$ of wild-type, Omicron variant and Delta variant were 18.6 %, 16.6 % and 15.4 %, respectively. The $\Delta F/F_0$ of SARS was 5.3 % due to its similar structure with SARS-CoV-2 [41]. As for MERS, a low $\Delta F/F_0$ of 1.3 % was obtained.

The detection of S protein in human serum was performed, and the concentration was calculated using the standard equation $y = 948651.0 + 65563.7\lg x$ (y is the fluorescence intensity, x is the concentration, ng/mL) in Fig. 5(b). The S protein was added in the serum and concentration were 0.1 ng/mL, 1 ng/mL and 10 ng/mL, respectively. The calculation results are shown in Table 2. Due to the matrix effect [42–44] caused by the complex components in the serum, the recovery was 110.05 %–115.45 % and the RSD was 10.84 %–13.30 %. The experimental results indicated this method can also detect S protein in actual serum.

4. Conclusions

In this paper, a novel FRET biosensor based on CQDs and AuNPs pairs was developed for detection of S protein of SARS-CoV-2. The fluorescence resonance energy transfer (FRET) would be generated when the CQDs and AuNPs serve as donor and acceptor. The positively charged ₊AuNPs and negatively charged ₋AuNPs were synthesized. Anti-SARS-CoV-2 spike RBD neutralizing antibody were modified on the surface of CQDs and AuNPs. The distance-based FRET theory was utilized to detect the spike (S) protein. Through the measurement of electric charge, it was found that using the negatively charged CQDs-Ab (antibody modified CQDs) and the positively charged ₊AuNPs could produce the best FRET effect due to the tightly adsorption. The limit of detection (LOD) of S protein is 0.05 ng/mL, the linear range is 0.1–100 ng/mL, and the detection process takes 12 min. For the Omicron variant (B.1.1.529) and the Delta variant (B.1.617.2), this method has a quite good detection effect. The recovery of S protein in human serum was in the range 110.05–115.45 %, and RSD was less than 13.30 %, this method was also feasible for serum S protein detection. Attribute to the easy operation and high specificity, this method has great potential for SARS-CoV-2 virus early diagnosis and preventing disease transmission.

Data availability statement

Data included in article/supplementary material/referenced in article.

CRediT authorship contribution statement

Yang Li: Conceptualization, Data curation, Formal analysis, Methodology, Writing – original draft. **Yashuang Ren:** Data curation, Formal analysis. **Zhihao Yi:** Investigation, Methodology. **Shitong Han:** Supervision, Validation. **Shilei Liu:** Data curation. **Feng Long:** Visualization. **Anna Zhu:** Conceptualization, Writing – review & editing.

Declaration of competing interest

The authors declare that they have no known competing financial interests or personal relationships that could have appeared to influence the work reported in this paper.

Appendix A. Supplementary data

Supplementary data to this article can be found online at https://doi.org/10.1016/j.heliyon.2023.e22674.

References

[1] R. Gaur, D.K. Verma, R. Mohindra, et al., Buccal swabs as non-invasive specimens for detection of severe acute respiratory syndrome coronavirus-2[J], J. Int. Med. Res. 49 (5) (2021), 03000605211016996.
[2] Q. Lin, D. Wen, J. Wu, et al., Microfluidic immunoassays for sensitive and simultaneous detection of IgG/IgM/Antigen of SARS-CoV-2 within 15 min[J], Anal. Chem. 92 (14) (2020) 9454–9458.
[3] G. Seo, G. Lee, M.J. Kim, et al., Rapid detection of COVID-19 causative virus (SARS-CoV-2) in human nasopharyngeal swab specimens using field-effect transistor-based biosensor[J], ACS Nano 14 (4) (2020) 5135–5142.
[4] Y.M. Bar-On, A. Flamholz, R. Phillips, et al., SARS-CoV-2 (COVID-19) by the numbers[J], Elife 9 (2020), e57309.
[5] J. Lan, J. Ge, J. Yu, et al., Structure of the SARS-CoV-2 spike receptor-binding domain bound to the ACE2 receptor[J], Nature 581 (7807) (2020) 215–220.
[6] W. Li, Z. Wei, B. Wang, et al., Carbon quantum dots enhanced the activity for the hydrogen evolution reaction in ruthenium-based electrocatalysts[J], Mater. Chem. Front. 4 (1) (2020) 277–284.
[7] Q. Wei, T. Liu, H. Pu, et al., Determination of acrylamide in food products based on the fluorescence enhancement induced by distance increase between functionalized carbon quantum dots[J], Talanta 218 (2020), 121152.
[8] H. Ehtesabi, Application of carbon nanomaterials in human virus detection[J], Journal of Science-Advanced Materials and Devices 5 (4) (2020) 436–450.
[9] L. Xu, Q. Zhang, S. Ding, et al., Ultrasensitive detection of severe fever with thrombocytopenia syndrome virus based on immunofluorescent carbon dots/SiO2 nanosphere-based lateral flow assay[J], ACS Omega 4 (25) (2019) 21431–21438.
[10] W. Li, Z. Wei, B. Wang, et al., Carbon quantum dots enhanced the activity for the hydrogen evolution reaction in ruthenium-based electrocatalysts[J], Mater. Chem. Front. 4 (1) (2020) 277–284.
[11] X. Li, Z. Wang, Y. Liu, et al., Bright tricolor ultrabroad-band emission carbon dots for white light-emitting diodes with a 96.5 high color rendering index[J], J. Mater. Chem. C 8 (4) (2020) 1286–1291.
[12] L. Tian, X. Zhai, X. Wang, et al., Morphology and phase transformation of alpha-MnO2/MnOOH modulated by N-CDs for efficient electrocatalytic oxygen evolution reaction in alkaline medium[J], Electrochim. Acta 337 (2020), 135823.
[13] L. Tian, J. Wang, K. Wang, et al., Carbon-quantum-dots-embedded MnO2 nanoflower as an efficient electrocatalyst for oxygen evolution in alkaline media[J], Carbon 147 (2019) 457–466.
[14] N. Li, L. Shi, X. Zou, et al., Fluorescence immunoassay rapid detection of 2019-nCoV antibody based on the fluorescence resonance energy transfer between graphene quantum dots and Ag@Au nanoparticle[J], Microchem. J. 173 (2022), 107046.
[15] H. Han, C. Wang, X. Yang, et al., Rapid field determination of SARS-CoV-2 by a colorimetric and fluorescent dual-functional lateral flow immunoassay biosensor [J], Sensor. Actuator. B Chem. 352 (2022), 130897.
[16] C. Li, Z. Zou, H. Liu, et al., Synthesis of polystyrene-based fluorescent quantum dots nanolabel and its performance in H5N1 virus and SARS-CoV-2 antibody sensing[J], Talanta 225 (2021), 122064.
[17] E. Deymehkar, M.A. Taher, C. Karami, et al., Synthesis of SPR nanosensor using gold nanoparticles and its application to copper (II) Determination[J], Silicon 10 (4) (2018) 1329–1336.
[18] N. Cennamo, L. Pasquardini, F. Arcadio, et al., SARS-CoV-2 spike protein detection through a plasmonic D-shaped plastic optical fiber aptasensor[J], Talanta 233 (2021), 122532.
[19] M. Zhang, X. Li, J. Pan, et al., Ultrasensitive detection of SARS-CoV-2 spike protein in untreated saliva using SERS-based biosensor[J], Biosens. Bioelectron. 190 (2021), 113421.
[20] Q. Zeng, Y. Zhang, X. Liu, et al., Multiple homogeneous immunoassays based on a quantum dots–gold nanorods FRET nanoplatform[J], Chem. Commun. 48 (12) (2012) 1781.
[21] L. Chang, X. He, L. Chen, et al., A fluorescent sensing for glycoproteins based on the FRET between quantum dots and Au nanoparticles[J], Sensor. Actuator. B Chem. 250 (2017) 17–23.
[22] I.L. Medintz, K.E. Sapsford, A.R. Clapp, et al., Designer variable repeat length polypeptides as scaffolds for surface immobilization of quantum dots[J], J. Phys. Chem. B 110 (22) (2006) 10683–10690.
[23] T. Pons, I.L. Medintz, K.E. Sapsford, et al., On the quenching of semiconductor quantum dot photoluminescence by proximal gold nanoparticles[J], Nano Lett. 7 (10) (2007) 3157–3164.
[24] G. Beane, K. Boldt, N. Kirkwood, et al., Energy transfer between quantum dots and conjugated dye molecules[J], J. Phys. Chem. C 118 (31) (2014) 18079–18086.
[25] G. Frens, Controlled nucleation for the regulation of the particle size in monodisperse gold suspensions[J], Nat. Phys. Sci. (Lond.) 241 (1973) 20–22.
[26] J. Zheng, H. Zhang, J. Qu, et al., Visual detection of glyphosate in environmental water samples using cysteamine-stabilized gold nanoparticles as colorimetric probe[J], Anal. Methods 5 (2013) 917.
[27] T. Niidome, K. Nakashima, H. Takahashi, et al., Preparation of primary amine-modified gold nanoparticles and their transfection ability into cultivated cells[J], Chem. Commun. (17) (2004) 1978–1979.
[28] R. Cao, B. Li, A simple and sensitive method for visual detection of heparin using positively-charged gold nanoparticles as colorimetric probes[J], Chem. Commun. 47 (10) (2011) 2865–2867.
[29] M.M. Alvarez, J.T. Khoury, T.G. Schaaff, et al., Optical absorption spectra of nanocrystal gold molecules[J], J. Phys. Chem. B 101 (19) (1997) 3706–3712.
[30] S. Link, Z.L. Wang, M.A. El-Sayed, Alloy formation of gold-silver nanoparticles and the dependence of the plasmon absorption on their composition[J], J. Phys. Chem. 103 (18) (1999) 3529–3533.
[31] G. Bharathi, F. Lin, L. Liu, et al., An all-graphene quantum dot Forster resonance energy transfer (FRET) probe for ratiometric detection of HE4 ovarian cancer biomarker[J], Colloids Surf. B Biointerfaces 198 (2021), 111458.
[32] Y. Chawre, M.L. Satnami, A.B. Kujur, et al., Forster resonance energy transfer between Multicolor emissive N-doped carbon quantum dots and gold nanorods for the detection of H_2O_2, glucose, glutathione, and acetylcholinesterase[J], ACS Appl. Nano Mater. 6 (9) (2023) 8046–8058.
[33] J. Korram, L. Dewangan, R. Nagwanshi, et al., A carbon quantum dot–gold nanoparticle system as a probe for the inhibition and reactivation of acetylcholinesterase: detection of pesticides[J], New J. Chem. 43 (18) (2019) 6874–6882.
[34] Y. Xu, C. Xia, X. Zeng, et al., Development of magnetic particle-based chemiluminescence immunoassay for measurement of SARS-CoV-2 nucleocapsid protein [J], J. Virol Methods 302 (2022), 114486.
[35] A.N. Baker, S.J. Richards, C.S. Guy, et al., The SARS-COV-2 spike protein binds sialic acids and enables rapid detection in a lateral flow point of care diagnostic device[J], ACS Cent. Sci. 6 (11) (2020) 2046–2052.
[36] A. Yakoh, U. Pimpitak, S. Rengpipat, et al., Paper-based electrochemical biosensor for diagnosing COVID-19: detection of SARS-CoV-2 antibodies and antigen [J], Biosens. Bioelectron. 176 (2021), 112912.
[37] H. Han, C. Wang, X. Yang, et al., Rapid field determination of SARS-CoV-2 by a colorimetric and fluorescent dual-functional lateral flow immunoassay biosensor [J], Sensor. Actuator. B Chem. 351 (2022), 130897.

[38] D. Liu, C. Ju, C. Han, et al., Nanozyme chemiluminescence paper test for rapid and sensitive detection of SARS-CoV-2 antigen[J], Biosens. Bioelectron. 173 (2021), 112817.
[39] S.L. Lee, J. Kim, S. Choi, et al., Fiber-optic label-free biosensor for SARS-CoV-2 spike protein detection using biofunctionalized long-period fiber grating[J], Talanta 235 (2021), 122801-122801.
[40] J.M. Lee, C.R. Kim, S. Kim, et al., Mix-and-read, one-minute SARS-CoV-2 diagnostic assay: development of PIFE-based aptasensor[J], Chem. Commun. 57 (79) (2021) 10222–10225.
[41] F. Wu, S. Zhao, B. Yu, et al., A new coronavirus associated with human respiratory disease in China[J], Nature 579 (7798) (2020) 265–269.
[42] F. Nasrin, A.D. Chowdhury, K. Takemura, et al., Single-step detection of norovirus tuning localized surface plasmon resonance-induced optical signal between gold nanoparticles and quantum dots[J], Biosens. Bioelectron. 122 (2018) 16–24.
[43] D. Song, J. Liu, W. Xu, et al., Rapid and quantitative detection of SARS-CoV-2 IgG antibody in serum using optofluidic point-of-care testing fluorescence biosensor[J], Talanta 235 (2021), 122800.
[44] J. Shi, C. Chan, Y. Pang, et al., A fluorescence resonance energy transfer (FRET) biosensor based on graphene quantum dots (GQDs) and gold nanoparticles (AuNPs) for the detection of mecA gene sequence of Staphylococcus aureus[J], Biosens. Bioelectron. 67 (2015) 595–600.